García Ivars, J.; Iborra Clar, MI.; Alcaina Miranda, MI.; Mendoza Roca, JA.; Pastor Alcañiz, L. (2014). Development of fouling-resistant polyethersulfone ultrafiltration membranes via surface UV photografting with polyethylene glycol/aluminum oxide nanoparticles. Separation and Purification Technology. 135:88-99. doi:10.1016/j.seppur.2014.07.056.

Development of fouling-resistant polyethersulfone ultrafiltration membranes via surface UV photografting with polyethylene glycol/aluminium oxide nanoparticles

Jorge Garcia-Ivars*[a], Maria-Isabel Iborra-Clar[a,b], Maria-Isabel Alcaina-Miranda[a,b], José-Antonio Mendoza-Roca[a,b], Laura Pastor-Alcañiz[c]

[a]Research Institute for Industrial, Radiophysical and Environmental Safety (ISIRYM), Universitat Politècnica de València, C/Camino de Vera s/n, 46022 Valencia, Spain

[b]Department of Chemical and Nuclear Engineering, Universitat Politècnica de València, C/Camino de Vera s/n, 46022 Valencia, Spain

[c]Depuración de Aguas de Mediterráneo, Avda. Benjamin Franklin, 21, Parque Tecnológico 46980 Paterna, Spain

Tel. +34 963879633

Fax. +34 963877639

Correspondence to: Jorge Garcia-Ivars (E-mail: *jorgariv@posgrado.upv.es*)

ABSTRACT

Polyethersulfone ultrafiltration membranes prepared via immersion precipitation with similar pore size were modified using UV irradiation with two nano-sized hydrophilic compounds of a different nature (an organic compound and a metal oxide). Effects of PEG/Al_2O_3 nanoparticles on membrane structure and the resulting performance were compared to determine the material with the best antifouling properties. Membranes were characterized by hydrophilicity (water contact angle, porosity, equilibrium water content and average pore radius), surface microscopic techniques (ATR-FTIR, SEM, EDX and AFM) and cross-flow ultrafiltration experiments (hydraulic permeability, membrane resistance and antifouling measurements). Membrane antifouling properties were analysed by several fouling/rinsing cycles using feed solutions of PEG of 35000 g

mol^{-1} with a concentration of 5 g L^{-1}. Water contact angle measurements, ATR-FTIR spectra, SEM images and EDX analysis indicated the presence of PEG/Al_2O_3 nanoparticles on the membrane surface. All UV-grafted membranes had higher hydraulic permeability than the unmodified membrane. Furthermore, polyethersulfone membranes photografted with 2.0 wt% PEG and 0.5 wt% Al_2O_3 displayed superior antifouling properties and desirable performance compared to all membranes tested. Therefore, this study proved that UV photografting of PEG/Al_2O_3 onto membrane surfaces is an appropriate technique for modifying polyethersulfone membranes to minimize membrane fouling.

KEYWORDS hydrophilicity; antifouling; photografting; ultraviolet irradiation; polyethylene glycol/aluminium oxide nanoparticles.

1. INTRODUCTION

Nowadays, ultrafiltration (UF) is a well-established membrane technology to separate water and microsolutes from macromolecules and colloids. UF membranes are used in a huge variety of applications, particularly in water production, chemicals processing, food processing, biotechnology, and wastewater treatment. These membranes are usually made from polymeric materials, though ceramic membranes are also available [1].

However, the contamination of a membrane, known as membrane fouling, is one of the most serious and inevitable problems in the UF membrane performance. Fouling depends on feed characteristics, operating parameters and membrane surface properties such as porosity, pore size, morphology, and hydrophilicity [2]. This phenomenon

remarkably reduces membrane performance due to the adsorption and deposition of solutes or particles onto the membrane surface or within its pores and hence, leads to an increase in hydraulic resistance during the filtration time. A higher hydraulic resistance is manifested as a decline in membrane permeation flux, which increases operating costs due to the need for frequent cleaning and maintenance, even replacement of the membrane [3]. In this way, many researchers have paid close attention to the study of the problems associated with membrane fouling. These studies focus on different areas such as fouling characterization and mechanism [4], fouling modelling [5], and fouling minimization. For this last purpose, several researchers have modified membrane characteristics to obtain a new material with better antifouling properties than the unmodified material. These unmodified materials are often high-performance UF membranes, which are made from polysulfone (PS) or polyethersulfone (PES) and are strongly fouled due to their low hydrophilic surface properties [6]. As a consequence, the improvement in membrane hydrophilicity is a good way to increase the fouling-resistant capability [7]. Membrane surface plays a determining role in permeation and separation properties because interactions between membrane and foulants take place mainly at the surface, while the porous sublayer provides the mechanical strength to the whole membrane structure.

Among the different existing techniques used in surface modification, photografting stands out as one interesting method to modify polymer membrane surfaces. In this technique, membranes are irradiated in the presence of monomer or any other additive in vapour or solution state. The irradiation source could be UV irradiation, X-ray irradiation, low temperature plasma, electron beam, etc [8]. However, UV irradiation is a very useful technique due to its relatively low investment cost, low temperature,

simple and rapid operation, and versatility. Moreover, modification via UV photografting produces a selective top-layer on the membrane surface due to a strong chemical bond to the substrate, which makes the membrane more mechanically stable under high operating pressure and preserves the mechanical properties of the base polymer [9].

This work deals with the modification of UF membranes made of PES by UV photografting. As PS, PES can easily generate free radicals when is irradiated by UV light, because of its inherent photosensitivity [10]. A recently method to enhance the membrane antifouling properties is using metal oxide nanoparticles on membrane structure and surface [11]. Among these metal oxide nanoparticles, nano-sized Al_2O_3 in gamma phase (γ-Al_2O_3) stands out due to their chemical inertness, availability, surface enrichment of reactive functional hydroxyl groups, mechanical strength and resistance to oxidation and corrosion [12].

The novelty of this work is the UV-modification of PES membranes by combining polyethylene glycol (PEG) of 400 g mol^{-1} and aluminium oxide (Al_2O_3) nanoparticles to improve antifouling properties. The aim is the introduction of both compounds in the surface structure of PES phase-inversion ultrafiltration membranes to minimize fouling. The surface properties and performance of all membranes were evaluated by Attenuated Total Reflectance Fourier Transform Infrared Spectroscopy (ATR-FTIR), Scanning Electron Microscopy (SEM), Energy Dispersive X-ray (EDX), Atomic Force Microscopy (AFM), membrane porosity, contact angle, hydraulic permeability, and fouling analysis.

2. EXPERIMENTAL

2.1 Materials

Polyethersulfone (PES, Ultrason E 6020 P, M_W = 51000 g mol^{-1}) was donated by BASF Co. (Germany). Nonwoven support was commercial grade Viledon FO 2431 from Freudenberg (Germany). N,N-Dimethylacetamide (DMA) was used as solvent in the phase-inversion method. Aluminium oxide (Al_2O_3) nanoparticles in gamma phase with primary particle size of 13 nm and a surface area of 100 m^2 g^{-1} (Sigma Aldrich, Germany) were used as the metal oxide. Polyethylene glycol of 400 g mol^{-1} (PEG 400) was provided by Sigma Aldrich (Germany), and was used as a water-soluble organic compound in UV-modification. Other researchers demonstrated that covalent bonding and grafting of PEG to other molecules may enhance their properties rendering them non-immunogenic, water soluble and protein rejecting. Das and Grupta investigated the degradation of PEG of different molecular weights using UV irradiation, showing that PEG is degraded at higher exposure time (2-7 h) than those used in this study (10 min, see in Chapter 2.3). Also, they demonstrated that PEGs with low molecular weight suffer lesser mass loss during UV irradiation than PEGs with high molecular weight. In addition, the hydrophilic nature of PEG 400 is such that water-hydrogen bonds with the polymer chain can inhibit protein absorption [13]. Therefore, PEG 400 can be a good choice as an organic compound in UV surface modification. PEG 400 and Al_2O_3 were selected to investigate the effects of the organic/inorganic nature on the membrane performance. Other types of polyethylene glycol (PEG 20000, and PEG 35000 from Sigma Aldrich, Germany; and PEG 10000 from Merck, Spain; the number indicates the different molar mass in g mol^{-1}) were also used as a part of the feed solution in membrane characterization. Deionized water was used throughout this study.

2.2. Membrane preparation

Phase-inversion method by immersion precipitation was applied for preparing asymmetric PES membranes. In this study, a homogeneous polymer solution with a composition of PES/DMA (20/80 wt%) was prepared under constant mechanical stirring at room temperature for at least 48 h. After that time, the polymer solution was then cast onto nonwoven supports by using a film applicator with a 75 μm casting knife, followed by immediate immersion in a coagulation bath of deionized water at room temperature to not allow a preceding dry phase-inversion in the atmosphere [14] and to remove the remaining solvent from the membrane structure. Once the coagulation process was finished, PES membranes were stored in deionized water until use. Prepared membranes with an approximate molecular weight cut-off of 30000 g mol^{-1} (30580 ± 2170 g mol^{-1}) were selected as base membranes for UV-modification. According to previous studies [15], MWCO of these membranes was obtained by sieving curves measured with PEG of different molecular weight in which solute rejection values were presented versus solute molecular weight. Thus, the smallest molecular weight at which 90% of rejection was obtained corresponded to membrane MWCO.

2.3. Surface modification

PES membranes were modified using the UV photografting equipment schematically represented in Fig. 1. An UV lamp of 6 W (Vilber Lourmat, France) is placed at the center of the ceil, providing uniform UV illumination (wavelength > 300 nm) over an area of up to 100 cm^2. PES membrane samples were immersed in grafting solutions (well-dispersed PEG/Al_2O_3 nanoparticles in aqueous solution) and they were covered with a glass UV filter. After 5 min since the first contact between the membrane and

grafting solutions, samples were subjected to UV irradiation for 10 min. In all experiments, reaction time was controlled by fixing the irradiation duration, the distance between the membrane surface and the UV lamp, and the relative humidity of the environment (40%). Thereafter, UV-grafted membranes were taken out and immediately rinsed with excess water to remove any unreacted compound and non-grafted chains from the membrane surface and pores. The washing process was sequentially done at room temperature for 30 min, at 50 ± 2 ºC for 2 h, and again at room temperature for 30 min. After washing, all the photografted membranes were stored in deionized water until use. The degree of modification or "degree of grafting" (*DG*) can be gravimetrically determined as the weight increase per membrane surface area as described by the following expression:

$$DG = \frac{(m_m - m_0)}{A} \qquad \text{Eq. (1)}$$

where m_0 is the initial membrane sample weight, m_m is the membrane weight after grafting modification, and *A* is the outer surface area of the membrane used.

All the membrane samples used for *DG* determination were not used for flux and fouling experiments because these measurements were destructive testing for the sample structure.

2.4 ATR-FTIR analysis

*A*ttenuated total reflection Fourier transform infrared spectroscopy (ATR-FTIR) was used to evaluate the chemical structure of the different membranes tested. ATR-FTIR spectra were measured on a Thermo Nicolet® Nexus spectrometer using a ZnSe crystal with a nominal incident angle of 45º. For each measurement, 128 scans were performed

for the range of 600-4000 cm^{-1}, with a resolution of 4 cm^{-1}. Membrane samples were dried in a vacuum oven overnight at room temperature before analysis.

2.5 Membrane porosity (ε) and equilibrium water content (EWC)

Membrane porosity (ε) and equilibrium water content (*EWC*) were studied to determine the degree of hydrophilicity or hydrophobicity of the membranes. After membranes were equilibrated in water, the volume occupied by water and the volume of the membranes in wet state were determined. Wet membranes were dried by putting in a vacuum oven for 24 h at 50 ºC and then they were weighed in dry state. Membrane porosity was obtained using the following equation [16]:

$$\varepsilon(\%) = \frac{\frac{(W_W - W_D)}{\rho_W}}{\frac{(W_W - W_D)}{\rho_W} + \frac{W_D}{\rho_p}} \cdot 100 \qquad \text{Eq. (2)}$$

where W_W is the weight of wet membranes (g), W_D is the weight of dry membranes (g), ρ_W is the density of pure water at operating conditions (g cm^{-3}), and ρ_p is the density of the polymer (g cm^{-3}).

EWC indicates the amount of water molecules that fill the membrane pores. *EWC* was estimated by Eq. (3):

$$EWC(\%) = \frac{W_W - W_D}{W_W} \cdot 100 \qquad \text{Eq. (3)}$$

These parameters are strongly related to hydraulic permeability and therefore have an important role on permeation and separation [17].

2.6 Average pore radius (r_m)

Membrane average pore radius (r_m) represents the average pore size along the membrane thickness (ζ) and is used to estimate the true membrane pore size. This parameter was determined by water filtration velocity method under constant transmembrane pressure (300 kPa) and it could be calculated by the Guerout-Elford-Ferry equation [18]:

$$r_m = \sqrt{\frac{(2.9 - 1.75 \cdot \varepsilon) \cdot (8 \cdot \mu \cdot \zeta \cdot Q_W)}{\varepsilon \cdot A_m \cdot \Delta P}} \quad \text{Eq. (4)}$$

where η is the water viscosity (Pa s), Q_W is the water flow (m^3 s^{-1}) and ΔP is the transmembrane pressure (MPa).

2.7 Contact angle measurement

Water contact angle was measured using an optical measurement system (Dataphysics OCA20, Germany) for predicting hydrophilicity. Three microlitres of deionized water were dropped on a dried flat membrane surface from a microsyringe with a stainless steel needle at room temperature conditions. Contact angle values were averaged from ten random locations for each membrane sample. If membranes are hydrophilic, the angle stays lower than 90º [19].

In order to study the stability of the hydrophilic PEG/Al_2O_3 nanoparticles incorporated on the membrane surface and its structure in a qualitative way, all membranes were soaked in water (25 ± 2 ºC). During 10 days of incubation time, WCA measurements were performed for each membrane and the variation of these measurements was used as the indicator of the photomodification stability. With this experiment, it can be confirmed if Al_2O_3 nanoparticles were well trapped in the grafted layer. This test was similar to that reported by Susanto et al. [20].

2.8 Membrane morphology

The cross-sectional morphology was observed by scanning electron microscopy (SEM). Cross-sections were obtained by breaking the membranes into small pieces. For this purpose, membrane samples were immersed in liquid nitrogen and all the samples were sputtered with a thin conductive layer of carbon, prior to SEM analysis. Energy dispersive X-ray spectroscopy (EDX) analysis was also performed to reveal the real composition of a certain part of the membrane. Both analyses were carried out with a scanning electron microscope and its adjunct EDX analyser (JEOL JSM6300 scanning microscope, Japan). Each reported value was expressed by the average of three measurements for each sample.

A multimode atomic force microscopy (VEECO Instruments (USA)) was also used to obtain the membrane surface roughness. All AFM images were obtained from 5 μm x 5 μm samples over different areas of each membrane. Also, these images were taken in ambient air in tapping mode, which is ideal for studying relatively soft samples such as grafted polymers [21]. Roughness values were obtained as the average of ten different areas of 1 μm x 1 μm for each membrane sample. The average roughness (S_a) and the root mean square roughness (S_q) were calculated by the following expression, considering a value for the parameter N (number of data points) of 512 [5]:

$$S_a = \frac{1}{N}\sum_{i=0}^{N}\left|Z_i - Z_{avg}\right| \qquad \text{Eq. (5)}$$

$$S_q = \sqrt{\frac{1}{N}\sum_{i=0}^{N}\left|Z_i - Z_{avg}\right|^2} \qquad \text{Eq. (6)}$$

where Z_{avg} is the average of the Z values within the given area, Z_i is the current Z value measured and N is the number of points within the given area.

247

248 *2.9 Membrane performance*

249 Membrane performance was studied in terms of hydraulic permeability, solute rejection
250 and fouling experiments. All experiments were conducted with an UF experimental
251 setup, which is described in a previous paper [22]. Initially, all membranes were
252 compacted at a transmembrane pressure (ΔP) of 100 kPa for 30 minutes, until the
253 difference between values of the permeate mass during the filtration time was lower
254 than 2%. Then, hydraulic permeability experiments were carried out with deionized
255 water at different transmembrane pressures (from 100 to 300 kPa), constant cross-flow
256 velocity (2.08 m s^{-1}) and 25 ºC. All deionized water fluxes (J_W) were measured by
257 gravimetric method until the values remained constant (with a difference lower than 5%
258 in periods of 6 min). J_W (L m^{-2} h^{-1}) was determined as follows:

259 $$J_W = \frac{V}{A_m \cdot t} \qquad \text{Eq. (7)}$$

260 where V is the total volume permeated (m^3) during the experimental time interval t (h)
261 and A_m is the effective surface area of the membrane (m^2).

262

263 Hydraulic permeability (P_h) was obtained from the slope of the plot of J_W and ΔP and
264 was calculated by:

265 $$P_h = \frac{J_W}{\Delta P} \qquad \text{Eq. (8)}$$

266

267 According to Darcy's law, membrane intrinsic resistance or membrane resistance (R_m)
268 was obtained using the following expression (Eq. (9)):

269 $$R_m = \frac{\Delta P}{\mu \cdot J_W} \qquad \text{Eq. (9)}$$

Rejection tests were conducted in the same above-mentioned UF setup using 1 g L^{-1} PEG solutions individually prepared with different molecular weights from 10000 to 35000 g mol^{-1}. The compositions of PEG solutions in the permeate stream (C_p) and in the feed/concentrate streams (C_f) were analysed using a high-precision Atago Refractometer (Atago RX-5000) at 20 °C within an accuracy of ± 0.00004 units. Rejection (R) was estimated by Eq. (10):

$$R(\%) = \left(1 - \frac{C_p}{C_f}\right) \cdot 100 \qquad \text{Eq. (10)}$$

After hydraulic permeability and solute rejection tests, dynamic permeation experiments via cross-flow ultrafiltration were performed using PEG of 35000 g mol^{-1} with a concentration of 5 g L^{-1} as a model foulant solution. PEG has been extensively used as a standard foulant in different UF experiments to study fouling behaviour and surface hydrophilic properties [23]. Each PES membrane was firstly subjected to a compaction test with deionized water at 200 kPa and constant cross-flow velocity (2.08 m s^{-1}) during 30 min and then, three cycles of fouling experiments with hydraulic cleaning (rinsing) were carried out for each membrane. Each filtration cycle included two steps: PEG solution filtration at 200 kPa for 2h and rinsing with deionized water for 30 min. These experiments were repeated three times. The permeate flux during PEG ultrafiltration J_f (L m^{-2} h^{-1}) and water flux during rinsing J_W (L m^{-2} h^{-1}) were measured by gravimetric method. In order to evaluate the membrane fouling-resistant capability, normalized flux ratio (NFR) was expressed as follows:

$$NFR(\%) = \left(\frac{J_{f2}}{J_{f1}}\right) \cdot 100 \qquad \text{Eq. (11)}$$

where J_{f1} and J_{f2} are the membrane fluxes at the beginning and after the fouling process, respectively. Generally, higher *NFR* values (next to 1) indicate better antifouling property of the membrane.

3. RESULTS AND DISCUSSION

3.1 Surface chemistry analysis by ATR-FTIR

In order to improve the hydrophilicity and the separation performance of PES membranes, UV-modification of PES membranes with four different PEG/Al_2O_3 concentrations were studied. Table 1 shows the different PEG/Al_2O_3 compositions in the grafting solution for each membrane studied. ATR-FTIR was employed to provide information about the chemical structure of all membranes. Fig. 2 presents the ATR-FTIR spectra of the modified PES membranes with varying PEG/Al_2O_3 contents. Additionally to all the membranes tested, two new samples were prepared to compare all the possible absorption peaks and bands appeared during ATR-FTIR spectra (UV-irradiated PES membrane without additives (PES/UV) and UV-grafted PES/PEG membrane without Al_2O_3 (PES/PEG)). It is also important to note that the PES/UV membrane was not included in the experimental design because the UV irradiation in the absence of monomer/additive solution degraded PES material and made this membrane unsuitable for the next tests.

All the membranes showed typical spectrum of PES material, aromatic bands at 1577 cm^{-1} and 1487 cm^{-1} from the benzene ring stretching and C-C bond stretching, respectively. Also, the absorption peak at 1242 cm^{-1} was assigned to the aromatic ether (C-O-C) stretching. The absorption band appeared at 1012 cm^{-1} could be attributed to the symmetric O=S=O stretching vibrations of sulfonated groups [24]. In the same way,

1323 cm^{-1}/1298 cm^{-1} doublet and 1151 cm^{-1} peak were assigned to the asymmetric and symmetric stretching of the aromatic sulfone chromophore, respectively [25].

Comparing the photomodified membranes with the unmodified membrane, a new absorption band appeared at 1647 cm^{-1}, which could be attributed to the carboxyl group (O-C=O) in asymmetrical stretching and appeared when PES was UV-grafted [24,26]. Also, new absorption peaks appeared (in a very low scale, but there are present in ATR-FTIR spectra) at 2920 cm^{-1} and 2852 cm^{-1}, which could be assigned to the asymmetric and symmetric stretching vibration of $–CH_2$. However, the low values of the intensity of these peaks made them barely perceptible in the ATR-FTIR spectra depicted in Fig. 2. There was no evidence that all these peaks (1647, 2852 and 2920 cm^{-1}) existed onto the unmodified PES membrane surface, so their appearance was related to the UV grafting process. These peaks had higher intensity when the presence of PEG on the membrane increased. The evidence of Al_2O_3 on the membrane surface was presented below. Two small peaks at 798 cm^{-1} and 1072 cm^{-1} were identified with the stretching vibration and the symmetric bending modes of Al-O-Al bonds, respectively. Likewise, the band observed at 623 cm^{-1} could be attributed to Al-O vibrations [27,28].

Finally, the small and characteristic broad band around 3300-3400 cm^{-1} could be attributed to the stretching of the hydroxyl group (O-H). However, there was no hydroxyl band in PES structure. Compared with the ATR-FTIR spectrum of PES/PEG samples, the presence of PEG chains with hydroxyl groups in the polymeric membrane structure may cause the appearance of this band. Moreover, the intensity of such band was slightly stronger when PEG content increased.

Therefore, these peaks indicated the presence of PEG/Al_2O_3 on the membrane surface and then, a successful photomodification of the PES membranes.

3.2 Degree of grafting

The effect of UV irradiation in the presence of different PEG/Al_2O_3 concentrations on PES membranes was analyzed using the degree of grafting (*DG*), and the results are presented in Table 1. For PES3 and PES4 membranes, the *DG* results included both PEG and Al_2O_3 nanoparticles contribution. *DG* increased with Al_2O_3 content, while the increasing rate of *DG* was considerably higher when PEG/Al_2O_3 was added due to the UV-induced grafting of hydrophilic PEG chains onto the PES membrane surface. In this process, hydrophilic γ-Al_2O_3 nanoparticles were entrapped on the surface structure, modifying the weight of polymer grafted on the membrane surface. This influence between the PEG content and the *DG* was also studied by other researchers [29]. The maximum value of *DG* (553.14 μg cm^{-2}) was obtained at a concentration of 4.5 wt% PEG and 0.5 wt% Al_2O_3 (PES4). With an increase in additives concentration during the UV irradiation, surface free radical had more chance to contact with PEG/Al_2O_3 and a higher DG was achieved. However, UV photografting on the surface structure was prevented due to the insufficient room for new polymer chains at high PEG concentration. Thus, the increasing rate of DG was slow at high PEG concentration [30].

3.3 Contact angle

Water contact angle (WCA) is an important parameter used to evaluate the surface hydrophilicity of a membrane. A high WCA value represents a hydrophobic surface, whereas a small WCA value implies a hydrophilic surface. Table 1 summarizes the

WCA results obtained for UF membranes before and after UV photografting. As expected, all the photomodified membranes had lower contact angles than the unmodified PES membrane (PES0), which possesses a hydrophobic surface [31]. So, PES0 exhibited the highest WCA (72.9 ± 1.5º), whereas 1 wt% Al_2O_3 photomodified PES membrane (PES2) presented the lowest WCA (49.9 ± 2.1º). These results indicated that the membrane became more hydrophilic with the presence of Al_2O_3 nanoparticles in its surface, due to their higher affinity for water than PES material [22]. While PEG incorporation on the membrane surface slightly entailed changes in the hydrophilic properties [32], the WCA values obtained for PES membranes photomodified with PEG/Al_2O_3 were higher than PES2. Therefore, the main responsible for the improvement of membrane surface hydrophilicity with increasing PEG/Al_2O_3 content is the high affinity for water from γ-Al_2O_3 nanoparticles and to a lesser extent the presence of hydrophilic functional groups from PEG 400.

Also, it was found that WCA showed a dependence on the values of DG. At the same Al_2O_3 concentration, when PEG was added, WCA decreased (from 59.8 to 53.9 and 51.9) as well as DG value increased (from 287.8 to 494.1 and 553.1). Strong dependence between WCA and DG can be seen when Al_2O_3 concentration increased. An intrinsic relationship between both parameters (DG and WCA) was obtained by Zhao et al. [7], who studied the changes in the hydrophilicity of polypropylene (PP) membrane surfaces after UV-induced graft polymerization using two oppositely charged monomers, [2-(methacryloyloxy)ethyl]trimethylammonium chloride (TM) and 3-sulfopropyl methacrylate potassium salt (SA). When membrane surfaces were entirely grafted with one monomer, authors obtained higher WCA than the WCA presented by the combination of both monomers.

Fig. 3 shows the results obtained for this stabilization test. WCA values of all modified membranes were higher with increasing the incubation time in water. After the incubation time, all modified membranes presented lower WCA values than those obtained for the unmodified membrane, which was an indication of the presence of Al_2O_3 nanoparticles on the surface structure and that they were stabilized and well secured. Comparing the modified membranes among themselves, PES membranes photomodified only with Al_2O_3 nanoparticles (PES1 and PES2) presented a higher increase in WCA values than PES membranes photomodified with PEG/Al_2O_3 (PES3 and PES4) during the incubation time. Therefore, Al_2O_3 nanoparticles could leach out from the membrane matrix after certain time, but the presence of PEG prevented the leaching of Al_2O_3 nanoparticles, causing a lower increase in WCA values during the incubation time and thus, a lower loss of Al_2O_3 nanoparticles.

3.4 Membrane porosity, equilibrium water content and average pore radius

Membrane porosity (ε) and Equilibrium water content (*EWC*) can be used for membrane characterization to determine the hydrophilicity of a membrane and their results are presented in Table 1. Firstly, all the membranes showed good porosity and *EWC* with values between 68 and 75%. It can be observed that the *EWC* percentage slightly increased after the photomodification process. *EWC* of the unmodified membrane was 68.52%, but it increased up to 71.44% when the presence of Al_2O_3 on the membrane surface increased up to 1 wt%. Furthermore, the presence of PEG/Al_2O_3 resulted in a more hydrophilic surface, increasing from 68.52 to 74.04% when the PEG content was 4.5 wt%. Therefore, the results showed that the UV photomodification with PEG/Al_2O_3 increased the hydrophilic character of PES membranes. Membrane porosity

418 presented the same trend. Similar behaviour was observed by Pulat and Babayigit,
419 whose research demonstrated that the *EWC* increased with the grafting of acrylamide
420 (AAm) and itaconic acid (IA) in polyurethane (PU) membranes by swelling
421 measurements [33].
422
423 Regarding the results shown in Table 1, the unmodified membrane had a relatively
424 larger mean pore size. However, the average pore size of the PES membrane decreased
425 when hydrophilic Al_2O_3 nanoparticles were grafted by UV irradiation onto the
426 membrane surface. Therefore, UV grafting reduced pore size [34]. However, the results
427 for PES membranes with PEG/Al_2O_3 are very interesting and noteworthy. At low PEG
428 concentration, an increase in PEG content caused a decrease in r_m, hence a smaller pore
429 size was obtained compared to the unmodified PES membrane. However, when higher
430 PEG concentrations were added onto the membrane surface, more open pores were
431 formed (r_m increased). These results are in agreement with the pore size studies
432 performed by Abu Seman et al. with acrylic acid in nanofiltration PES membranes. At
433 low monomer concentration, some molecules penetrated into the membrane pores
434 during the immersion process and then were photografted by UV light. During the UV
435 irradiation, these molecules indirectly narrowed the membrane pores. At higher
436 monomer concentration, a more compact membrane matrix could be developed, what
437 minimized the amount of grafted additive and its penetration inside the pores [35].
438
439 *3.5 Scanning electron microscopy (SEM)*
440 Microscopic study through SEM analysis was used to have qualitative information
441 about the influence of the photomodification on the membrane structure. The cross-
442 section morphology of the membranes was observed using SEM and these images are

presented in Fig. 4. The unmodified membrane (PES0) exhibited typical asymmetric structure consisting of a compact top layer and a porous finger-like substructure. The formation of this structure by phase-inversion method and its inherent phenomena had been explained by previous researchers [36]. Also, this membrane had a smoother and more homogeneous surface and apparently a larger porosity than all photomodified membranes. Compared with unmodified PES, both pore narrowing and pore blocking were observed as consequences of the UV photografted surface [31]. These effects were more pronounced for UV-modification using only Al_2O_3. PES membranes photomodified with Al_2O_3 (PES1 and PES2) presented an irregular and smaller finger-like structure with little agglomerations of Al_2O_3 nanoparticles entrapped in the pore channels because UV grafting can occur a certain depth into the membrane structure, not only in the outer membrane surface. Saha et al. [37] demonstrated that photomodification will not completely be limited to the outer membrane surface because both additives and UV irradiation could penetrate into the membrane pores. For higher Al_2O_3 concentration in the UV-grafted membrane (PES2), modification resulted in a rougher structure. PEG/Al_2O_3 photomodified membranes (PES3 and PES4) and PES0 had very similar morphologies [38], except that a larger finger-like structure was observed below the skin layer of the PES/PEG/Al_2O_3 membranes. Furthermore, there was no evidence of Al_2O_3 agglomerations in pore channels near the membrane surface, which may be due to the fact that PEG reoriented the Al_2O_3 nanoparticles on the membrane surface during UV photografting. Therefore, the heterogeneous appearance of PEG/Al_2O_3 UV-grafted surfaces is another proof of grafting.

3.6 Energy dispersive X-ray spectroscopy (EDX)

Simultaneously to SEM technique, EDX analysis was performed to investigate the distribution of Al_2O_3 nanoparticles as well as the effect of the photomodification on membrane surfaces. This technique is useful to corroborate the results obtained by ATR-FTIR spectroscopy. Table 2 shows the EDX results of unmodified and photomodified membranes. EDX results demonstrated the presence of C, O, S for all the membranes, including Al element for all the photomodified membranes, which gave evidence of the efficiency of UV photografting using Al_2O_3 nanoparticles. When PES membranes with Al_2O_3 nanoparticles were UV irradiated, the presence of Al element in the surface structure increased. This increment was higher when Al_2O_3 content in the grafting solution was increased. Therefore, Al_2O_3 nanoparticles were uniformly distributed on the whole membrane surface; however, some particles formed larger agglomerations. On the other hand, the presence of Al element decreased when PEG was added in the grafting solution, because Al_2O_3 nanoparticles were entrapped on the nascent surface structure during the UV-induced polymerization between PEG and PES. So, the presence of C element increased (present in the structure of PEG and PES) and the presence of S element and Al element (only present in PES structure and in Al_2O_3 structure, respectively) decreased. There is not much difference between the results obtained for PES3 and PES4.

3.7 Atomic force microscopy (AFM)

AFM analyses were performed to investigate the surface morphology at a nanoscopic scale and quantify the surface roughness of a membrane. Fig. 5 provides the three-dimensional AFM images of the PES membranes before and after modification for a scale of 1 μm x 1 μm. The brightest area presents the highest points of the membrane surface and the dark regions illustrate valleys or membrane pores. It can be seen that the

unmodified membrane showed a flatter surface than photomodified membranes. Table 1 indicates the calculated roughness of the membrane surfaces. AFM results showed that the membrane surface had a higher roughness after UV photomodification [37]. Compared with WCA results, an improvement in hydrophilicity suggested that the surface roughness of UV-grafted membranes would be greater compared to unmodified PES membrane [26]. The average roughness of the membranes (S_a) slightly increased from 3.43 nm to 3.87 nm when Al_2O_3 was grafted. When Al_2O_3 content was 1.0 wt% (PES2), S_a dramatically increased to 8.43 nm, which was the highest value of S_a observed in all the membranes tested. This phenomenon may be due to the fact that PES is a photosensitive polymer material to UV light [39]. When PES membranes were irradiated ($\lambda \approx 300$ nm) in the presence of Al_2O_3, their own polymer chains could be cleaved and then, their surface structure was weakened. In this moment, Al_2O_3 nanoparticles could be deposited onto the membrane surface, in which these nanoparticles were entrapped onto the surface polymer chains (PES). The weakening of the PES surface structure could be avoided at longer wavelength UV light ($\lambda > 350$ nm) [40].

In the same way, S_a barely increased from 3.43 nm to 3.59 nm when PEG content was 2.0 wt%. However, at high PEG concentration (4.5 wt%), the value of S_a increased to 7.29 nm. Therefore, the surface roughness increased when the PEG concentration increased. In this case, UV irradiation activated the PES membrane surface, which formed polymer chains with the PEG reacted and entrapped Al_2O_3 nanoparticles in the nascent surface structure. This UV-induced polymerization made the membrane surface rougher.

3.8 Ultrafiltration performances

The effect of UV photografting on the performance of the PES membranes was investigated by using pure water and PEG filtration. Table 3 shows the effect of the different PEG/Al_2O_3 grafting solutions on the membrane hydraulic permeability and the membrane intrinsic resistance.

Hydraulic permeability of the unmodified PES membrane was slightly increased by UV photografting using hydrophilic compounds onto the PES membrane surface. When Al_2O_3 content in the grafting solution was higher, hydraulic permeability increased due to the hydrophilic nature of the Al_2O_3 nanoparticles as well as the homogeneity of its presence in the membrane surface structure [22]. This increment was also attributed to the higher DG and membrane surface roughness and pore structure. The increase in hydraulic permeability was higher when hydrophilic PEG 400 was present in the grafting solution. Even though photografting generally reduces pore size, enhancement in hydraulic permeability may be explained by the introduction of polar groups and the formation of larger pores, due to the high affinity of water molecules to the hydrophilic PEG chains onto the membrane [38]. For UV-irradiated PES membranes with 2.0 wt% PEG and 0.5 wt% Al_2O_3, hydraulic permeability increased from 2.352 L m^{-2} h^{-1} kPa^{-1} to 3.145 L m^{-2} h^{-1} kPa^{-1}. However, the highest hydraulic permeability (3.575 L m^{-2} h^{-1} kPa^{-1}) was observed by UV-irradiated PES membranes with 4.5 wt% PEG and 0.5 wt% Al_2O_3, most probably as a result of larger pore sizes and pore density [25]. Consequently, the combined addition of PEG/Al_2O_3 resulted in a high hydraulic permeability and a low membrane resistance.

Solute rejection test were performed using 1 g L^{-1} PEG solutions with different molecular weights (10000, 20000 and 35000 g mol^{-1}). PEG rejections for membranes before and after modification were presented in Table 3. All the modified membranes had higher rejection for PEG solutions than the unmodified PES membrane. At the same Al_2O_3 concentration (PES1, PES3 and PES4), higher PEG 400 concentration caused an increase in PEG rejection, indicating an improvement in organic solute rejection when PEG/Al_2O_3 nanoparticles were added. The highest PEG rejections were obtained at the highest Al_2O_3 concentration tested (PES2). Such increment in solute rejection was an indication of smaller surface pore sizes in the photomodified membrane, which was confirmed by the average pore radius (r_m) results in Section 3.4. Therefore, these results indicate that the organic solute rejection of PES membranes enhanced once PEG/Al_2O_3 nanoparticles were grafted by UV irradiation on the membrane surface.

In order to evaluate the antifouling properties of the UV photomodified membranes, a compaction test with deionized water and then, three cycles of fouling/rinsing ultrafiltration were carried out. Results for PES membranes photografted with Al_2O_3 are shown in Fig. 6. During membrane compaction with deionized water, initial fluxes for PES membranes photografted with Al_2O_3 (PES1 and PES2) were higher than that of unmodified PES membrane (PES0). Moreover, photomodified membranes with Al_2O_3 nanoparticles were more affected by the compaction process than the unmodified one (losing about 5% of initial water flux more than PES0 during the compaction time). After all the fouling/rinsing experiments, total flux losses of all photomodified membranes with Al_2O_3 were slightly lower in comparison with the unmodified PES membrane. PES membrane with 1 wt% Al_2O_3 (PES2) exhibited the highest flux

recovery with a final flux value of 528.49 L m^{-2} h^{-1} (75% of the initial value). This phenomenon indicates that membranes photografted with Al_2O_3 had lower solute affinity, which could be caused by an improvement in PES membrane hydrophilicity by introducing hydrophilic Al_2O_3 nanoparticles, which could restrain the solute adsorption and deposition on the membrane surface [41].

Fig. 7 presented the results for PES membranes photografted with PEG/Al_2O_3. As it was seen for membranes photomodified with Al_2O_3 during the membrane compaction, the initial fluxes for PES membranes photografted with PEG/Al_2O_3 were higher than the initial fluxes of PES0. However, these membranes presented lower flux loss during membrane compaction (losing about 9% of the initial water flux value) than PES membranes photografted with Al_2O_3 (losing about 12% of the initial flux value). Moreover, all photografted PES membranes showed a higher flux recovery in comparison with PES0, especially UV-grafted PES membrane using 2 wt% PEG and 0.5 wt% Al_2O_3 (PES3) with a final flux value of 387.85 L m^{-2} h^{-1} (82% of the initial value). When the membrane surface and pore walls became more hydrophilic, membrane fouling was retarded due to a higher hydrophilicity caused by the combined effect of the PEG/Al_2O_3 nanoparticles on the grafted surface structure. Both additives had high affinity to polar components as water which led to a higher permeability for pure water and then, a high rejection to hydrophobic compounds such as proteins and macromolecules [42].

Finally, normalized flux ratio (NFR) was used to analyze the fouling degree of all the membranes prepared. The evolution of the parameter normalized flux ratio (NFR) with filtration time (2 h) was shown in Fig. 8. It was observed that all the photomodified

membranes exhibited less fouling tendency (higher NFR values) compared to the unmodified membrane (PES0), which is an indicator of the success in the alteration in membrane surface properties. PES3 showed the highest NFR values (81%), suffering the lowest total flux loss during ultrafiltration in comparison with the other membranes tested. Differences between the membrane performance of PES3 and PES4 could be related to the high PEG content in PES4. Previous studies about the surface graft modification of PES ultrafiltration membranes suggested that there is a certain monomer/additive concentration (PEG in our case) at which the maximum fouling resistance could be achieved, and further addition of this monomer was extraneous [29]. Thus, an increase in PEG content up to a certain value caused an increase in DG values but not an improvement in its permselective properties. As a consequence, PES membranes photomodified with PEG/Al_2O_3 nanoparticles (≈ 2 wt% PEG) reduced the hydrophobic interaction between PES membrane surface and foulants and therefore, the antifouling properties of PES membranes were improved by photochemical grafting of PEG monomer and Al_2O_3 nanoparticles.

4. CONCLUSIONS

Hydrophilized PES membranes were prepared via immersion precipitation and modified by UV irradiation in the presence of two different hydrophilic compounds (a metal oxide and a water-soluble monomer) to enhance the fouling-resistant capability of the membrane surface. The effect of PEG of 400 g mol^{-1} and Al_2O_3 at various concentrations on the morphology, performance and membrane structure were elucidated. The following conclusions have been derived from this study:

(1) PES membrane hydrophilicity was significantly increased by UV photografting with PEG/Al_2O_3 nanoparticles.

(2) The incorporation of the hydrophilic compounds on PES membranes during the UV grafting process was confirmed by ATR-FTIR, SEM, EDX and AFM analyses, in which chemical and morphological changes on membrane surface before and after modification were observed.

(3) Degree of grafting, membrane porosity and *EWC* increased with higher PEG/Al_2O_3 concentration.

(4) Pore size and water contact angle of the PES membranes decreased with UV photografting, implying an improvement of membrane surface hydrophilicity. Also, stabilization test by water contact angle measurements demonstrated that PEG could suppress the leaching of Al_2O_3 nanoparticles.

(5) Hydraulic permeability of all the modified membranes increased after the photomodification process.

(6) PEG permeation and rejection of PES membranes improved with UV photografting and therefore, their antifouling properties and flux recovery. The best results were obtained for PES membranes photografted with 2 wt% PEG/0.5 wt% Al_2O_3 nanoparticles.

5. ACKNOWLEDGEMENTS

The authors of this work thank the financial support of CDTI (Centre for Industrial Technological Development) depending on the Spanish Ministry of Science and Innovation. The authors also thank the Center for Biomaterials and Tissue Engineering (Universitat Politècnica de València) for ATR-FTIR and contact angle measurements and BASF (Germany) for supplying the polymers used.

6. REFERENCES AND NOTES

641 [1] R.W. Baker. Membrane Technology and Applications, second ed., John Wiley &
642 Sons Ltd., Chichester, 2004.
643 [2] D.B. Mosqueda-Jimenez, R.M. Narbaitz, T. Matsuura, G. Chowdhury, G. Pleizier,
644 J.P. Santerre, Influence of processing conditions on the properties of ultrafiltration
645 membranes, J. Membr. Sci. 231 (2004) 209-224.
646 [3] K.C. Khulbe, C. Feng, T. Matsuura, The art of surface modification of synthetic
647 polymeric membranes, J. Appl. Polym. Sci. 115 (2010) 855-895.
648 [4] S. Nataraj, R. Schomäcker, M. Kraume, I.M. Mishra, A. Drews, Analyses of
649 polysaccharide fouling mechanisms during crossflow membrane filtration, J. Membr.
650 Sci. 308 (2008) 152-161.
651 [5] M.-J. Corbatón-Báguena, S. Álvarez-Blanco, M.-C. Vincent-Vela, Cleaning of
652 ultrafiltration membranes fouled with BSA by means of saline solutions, Sep. Purif.
653 Technol. 125 (2014) 1-10.
654 [6] B.S. Lalia, V. Kochkodan, R. Hashaikeh, N. Hilal, A review on membrane
655 fabrication: structure, properties and performance relationship, Desalination 326 (2013)
656 77-95.
657 [7] Y-H. Zhao, X-Y. Zhu, K-H. Wee, R. Bai, Achieving highly effective non-biofouling
658 performance for polypropylene membranes modified by UV-induced surface graft
659 polymerization of two oppositely charged monomers, J. Phys. Chem. B 114 (2010)
660 2422-2429.
661 [8] C. Zhao, J. Xue, F. Ran, S. Sun, Modification of polyethersulfone membranes – a
662 review of methods, Prog. Mater. Sci. 58 (2013) 76-150.
663 [9] P.S. Zhong, N. Widjojo, T.-S. Chung, M. Weber, C. Maletzko, Positively charged
664 nanofiltration (NF) membranes via UV grafting on sulfonated polyphenylenesulfone

665 (sPPSU) for effective removal of textile dyes from wastewater, J. Membr. Sci. 417-418
666 (2012) 52-60.
667 [10] G. Xueli, W. Haizeng, W. Jian, H. Xing, G. Congjie, Surface-modified PSf UF
668 membrane by UV-assisted graft polymerization of capsaicin derivative moiety for
669 fouling and bacterial resistance, J. Membr. Sci. 445 (2013) 146-155.
670 [11] J.M. Arsuaga, A. Sotto, G. del Rosario, A. Martínez, S. Molina, S.B. Teli, J. de
671 Abajo, Influence of the type, size, and distribution of metal oxide particles on the
672 properties of nanocomposite ultrafiltration membranes, J. Membr. Sci. 428 (2013) 131-
673 141.
674 [12] M.R. Karim, M.A. Rahman, M.A.J. Miah, H. Ahmad, M. Yanagisawa, M. Ito,
675 Synthesis of γ-Alumina particles and surface characterization, Open Colloid Sci. J. 4
676 (2011) 32-36.
677 [13] I. Das, S.K. Gupta, Polyethylene glycol degradation by UV irradiation, Indian J.
678 Chem. 44A (2005) 1355-1358.
679 [14] C. Barth, M.C. Gonçalves, A.T.N. Pires, J. Roeder, B.A. Wolf, Asymmetric
680 polysulfone and polyethersulfone membranes: effects of thermodynamic conditions
681 during formation on their performance, J. Membr. Sci. 169 (2000) 287-299.
682 [15] L. Puro, M. Kallioinen, M. Mänttäri, G. Natarajan, D.C. Cameron, M. Nyström,
683 Performance of RC and PES ultrafiltration membranes in filtration of pulp mill process
684 waters, Desalination 264 (2010) 249-255.
685 [16] E. Yuliwati, A.F. Ismail, Effect of additives concentration on the surface properties
686 and performance of PVDF ultrafiltration membranes for refinery produced wastewater
687 treatment, Desalination 273 (2011) 226-234.
688 [17] B. Chakrabarty, A.K. Ghoshal, M.K. Purkait, Effect of molecular weight of PEG
689 on membrane morphology and transport properties, J. Membr. Sci. 309 (2008) 209-221.

690 [18] G. Wu, S. Gan, L. Cui, Y. Xu, Preparation and characterization of PES/TiO_2
691 composite membranes, Appl. Sur. Sci. 254 (2008) 7080-7086.
692 [19] A. Ananth, G. Arthanareeswaran, H. Wang, The influence of tetraethylorthosilicate
693 and polyethyleneimine on the performance of polyethersulfone membranes,
694 Desalination 287 (2012) 61-70.
695 [20] H. Susanto, A. Roihatin, N. Aryanti, D.D. Anggoro, M. Ulbricht, Effect of
696 membrane hydrophilization on ultrafiltration performance for biomolecules separation,
697 Materials Science and Engineering C 32 (2012) 1759-1766.
698 [21] W. Yoshida, Y. Cohen, Topological AFM characterization of graft polymerized
699 silica membranes, J. Membr. Sci. 215 (2003) 249-264.
700 [22] J. García-Ivars, M.-I. Alcaina-Miranda, M.-I. Iborra-Clar, J.-A. Mendoza-Roca, L.
701 Pastor-Alcañiz, Enhancement in hydrophilicity of different polymer phase-inversion
702 ultrafiltration membranes by introducing PEG/Al_2O_3 nanoparticles, Sep. Purif. Technol.
703 128 (2014) 45-57.
704 [23] Y. Kim, D. Rana, T. Matsuura, W.-J. Chung, Influence of surface modifying
705 macromolecules on the surface properties of poly(ether sulfone) ultra-filtration
706 membranes, J. Membr. Sci. 338 (2009) 84-91.
707 [24] S. Belfer, R. Fainchtain, Y. Purinson, O. Kedem, Surface characterization by
708 FTIR-ATR spectroscopy of polyethersulfone membranes-unmodified, modified and
709 protein fouled, J. Membr. Sci. 172 (2000) 113-124.
710 [25] H. Hua, N. Li, L. Wu, H. Zhong, G. Wu, Z. Yuan, X. Lin, L. Tang, Anti-fouling
711 ultrafiltration membrane prepared from polysulfone-graft-methyl acrylate copolymers
712 by UV-induced grafting method, J. Environ. Sci. 20 (2008) 565-570.

713 [26] A. Rahimpour, UV photo-grafting of hydrophilic monomers onto the surface of
714 nano-porous PES membranes for improving surface properties, Desalination 265 (2011)
715 93-101.
716 [27] U.O. Akkaya Arier, F.Z. Tepehan, Influence of Al_2O_3:TiO_2 ratio on the structural
717 and optical properties of TiO_2-Al_2O_3 nano-composite films produced by sol gel method,
718 Composites: Part B 58 (2014) 147-151.
719 [28] M.A. Ahmed, M.F. Abdel-Messih, Structural and nano-composite features of TiO_2-
720 Al_2O_3 powders prepared by sol-gel method, J. Alloy. Compd 509 (2011) 2154-2159.
721 [29] P.S. Yune, J.E. Kilduff, G. Belfort, Fouling-resistant properties of a surface-
722 modified poly(ether sulfone) ultrafiltration membrane grafted with poly(ethylene
723 glycol)-amide binary monomers, J. Membr. Sci. 377 (2011) 159-166.
724 [30] H. Yu, Y. Cao, G. Kang, J. Liu, M. Li, Q. Yuan, Enhancing antifouling property of
725 polysulfone ultrafiltration membrane by grafting zwitterionic copolymer via UV-
726 initiated polymerization, J. Membr. Sci. 342 (2009) 6-13.
727 [31] H. Susanto, M. Ulbricht, Photografted thin polymer hydrogel layers on PES
728 ultrafiltration membranes: characterization, stability, and influence on separation
729 performance, Langmuir 23 (2007) 7818-7830.
730 [32] W. Chinpa, D. Quémener, E. Bèche, R. Jiraratananon, A. Deratani, Preparation of
731 poly(etherimide) based ultrafiltration membrane with low fouling property by surface
732 modification with poly(ethylene glycol), J. Membr. Sci. 365 (2010) 89-97.
733 [33] M. Pulat, D. Babayigit, Surface modification of PU membranes by graft
734 copolymerization with acrylamide and itaconic acid monomers, Polym. Test. 20 (2001)
735 209-216.

[34] C. Emin, J.-C. Remigy, J.-F. Lahitte, Influence of UV grafting conditions and gel formation on the loading and stabilization of palladium nanoparticles in photografted polyethersulfone membrane for catalytic reactions, J. Membr. Sci. 455 (2014) 55-63.

[35] M.N. Abu Seman, M. Khayet, N. Hilal, Comparison of two different UV-grafted nanofiltration membranes prepared for reduction of humic acid fouling using acrylic acid and N-vinylpyrrolidone, Desalination 287 (2012) 19-29.

[36] I.M. Wienk, R.M. Boom, M.A.M. Beerlage, A.M.W. Bulte, C.A. Smolders, H. Strathmann, Recent advances in the formation of phase inversion membranes made from amorphous or semi-crystalline polymers, J. Membr. Sci. 113 (1996) 361-371.

[37] N.K. Saha, M. Balakrishnan, M. Ulbricht, Fouling control in sugarcane juice ultrafiltration with surface modified polysulfone and polyethersulfone membranes, Desalination 249 (2009) 1124-1131.

[38] T. Yuan, J. Meng, X. Gong, Y. Zhang, M. Xu, Modulating pore size and surface properties of cellulose microporous membrane via thio-ene chemistry, Desalination 328 (2013) 58-66.

[39] B. Kaeselev, J. Pieracci, G. Belfort, Photoinduced grafting of ultrafiltration membranes: comparison of poly(ether sulfone) and poly(sulfone), J. Membr. Sci. 194 (2001) 245-261.

[40] Y. Li, H. Zhang, H. Zhang, J. Cao, W. Xu, X. Li, Hydrophilic porous poly(sulfone) membranes modified by UV-initiated polymerization for vanadium flow battery application, J. Membr. Sci. 454 (2014) 478-487.

[41] L.-J. Zhu, L.-P. Zhu, J.-H. Jiang, Z. Yi, Y.-F. Zhao, B.-K. Zhu, Y.-Y. Xu, Hydrophilic and anti-fouling polyethersulfone ultrafiltration membranes with poly(2-hydroxyethyl methacrylate) grafted silica nanoparticles as additive, J. Membr. Sci. 451 (2014) 157-168.

[42] M. Peyravi, A. Rahimpour, M. Jahanshahi, A. Javadi, A. Shockravi, Tailoring the surface properties of PES ultrafiltration membranes to reduce the fouling resistance using synthesized hydrophilic copolymer, Microp. Mesop. Mater. 160 (2012) 114-125.

7. LIST OF SYMBOLS

Variables

A	Outer surface area of the membrane (cm^2)
A_m	Effective area of the membrane (m^2)
C_f	Concentration of PEG in feed stream (wt%)
C_P	Concentration of PEG in permeate stream (wt%)
DG	Degree of grafting ($\mu g\ cm^{-2}$)
EWC	Equilibrium water content
J	Steady-state permeate flux ($L\ m^{-2}\ h^{-1}$)
J_f	Permeate flux during PEG ultrafiltration ($L\ m^{-2}\ h^{-1}$)
J_{f1}	Permeate flux of the membranes obtained at the beginning of each fouling cycle ($L\ m^{-2}\ h^{-1}$)
J_{f2}	Permeate flux of the membranes after the fouling process ($L\ m^{-2}\ h^{-1}$)
J_p	Permeate flux ($L\ m^{-2}\ h^{-1}$)
J_W	Permeate water flux of the tested membranes ($L\ m^{-2}\ h^{-1}$)
m_0	Initial membrane sample weight (g)
m_m	Membrane weight after photografting process (g)
M_W	Molecular weight (Da)
N	Number of points within the given area (dimensionless)
NFR	Normalized flux ratio (%)
P_h	Hydraulic permeability ($L\ m^{-2}\ h^{-1}\ kPa^{-1}$)

Q_W	Water flow ($m^3\ s^{-1}$)
r_m	Average pore radius (m)
R	Solute rejection (%)
R_m	Membrane intrinsic resistance (m^{-1})
S_a	Average roughness (nm)
S_q	Root mean square roughness (nm)
t	Experimental time interval (h)
T	Feed temperature (°C)
V	Total volume permeated during an experimental time interval (L)
W_D	Weight of dry membranes (g)
W_W	Weight of wet membranes (g)
Z	Height values of the surface sample (nm)
Z_{avg}	Average of the Z values of the sample (nm)
Z_i	Z value currently measured (nm)
ΔP	Transmembrane pressure (MPa)

Greek letters

ε	Membrane porosity (%)
ζ	membrane thickness (m)
μ	Dynamic water viscosity (Pa s)
ρ_p	Density of the polymer ($g\ cm^{-3}$)
ρ_W	Density of pure water at operating conditions ($g\ cm^{-3}$)

Abbreviations

AAm	Acrylamide

811	AFM	Atomic force microscopy
812	ATR-FTIR	Attenuated total reflectance Fourier transform infrared spectroscopy
813	DMA	N,N-Dimethylacetamide
814	EDX	Energy dispersive X-ray
815	IA	Itaconic acid
816	PEG	Polyethylene glycol
817	PES	Polyethersulfone
818	PP	Polypropylene
819	PS	Polysulfone
820	PU	Polyurethane
821	SA	3-sulfopropyl methacrylate potassium salt
822	SEM	Scanning electron microscopy
823	TM	2-(methacryloyloxy)ethyl]trimethylammonium chloride
824	UF	Ultrafiltration
825	UV	Ultraviolet
826	WCA	Water contact angle

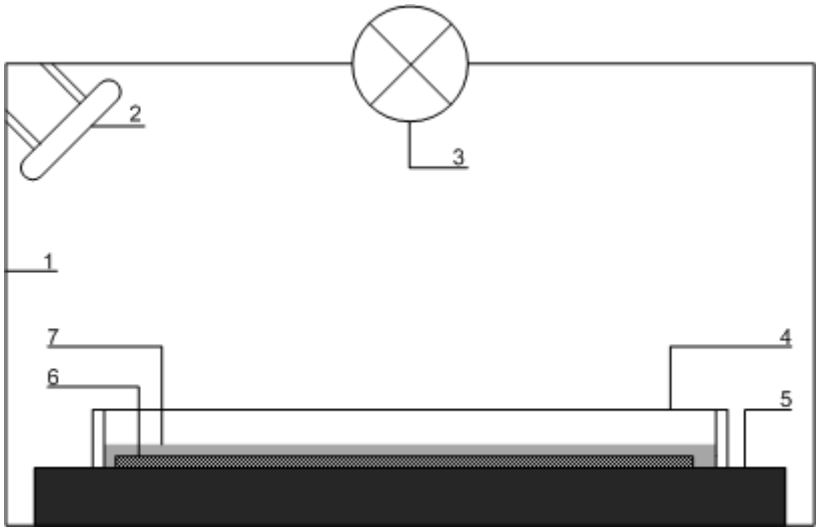

Fig. 1. Scheme of the UV-grafting equipment: 1, container; 2, mechanical fun; 3, UV lamp; 4, glass UV filter; 5, stainless steel support; 6, membrane; 7, grafting solution.

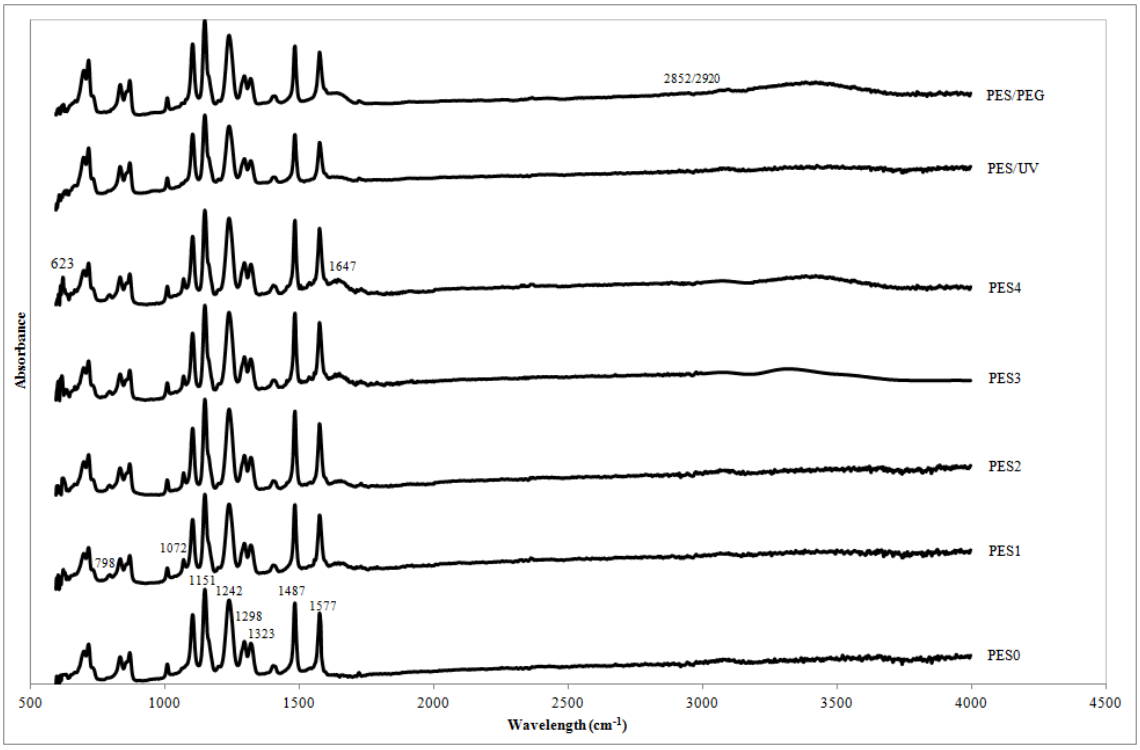

Fig. 2. FTIR-ATR spectra of PES membrane surfaces for different PEG/Al_2O_3 content.

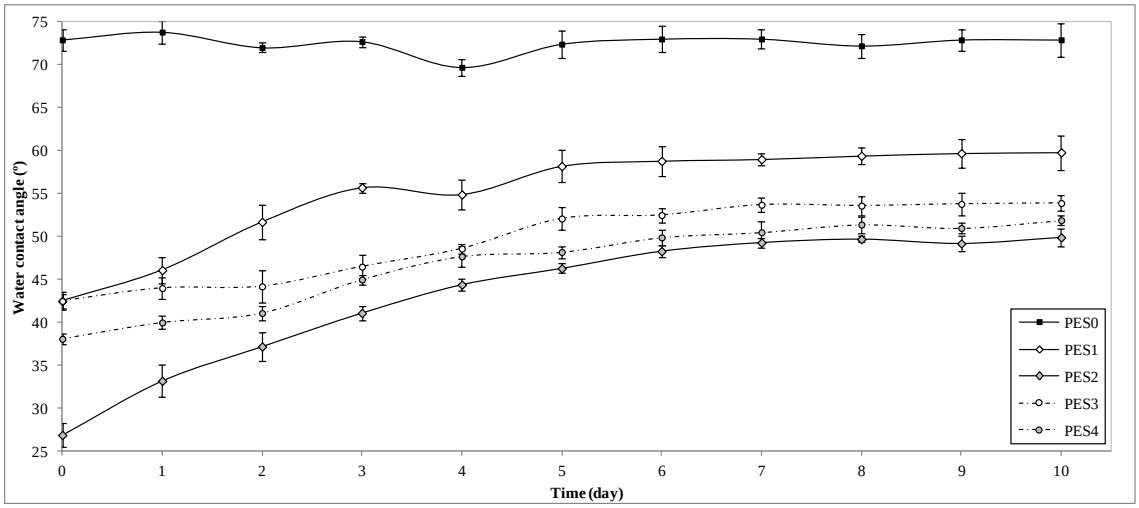

Fig. 3. Stability examination of different photomodification additive solutions investigated by measuring the water contact angle as a function of incubating time. Membranes were soaked in water at 25 ºC.

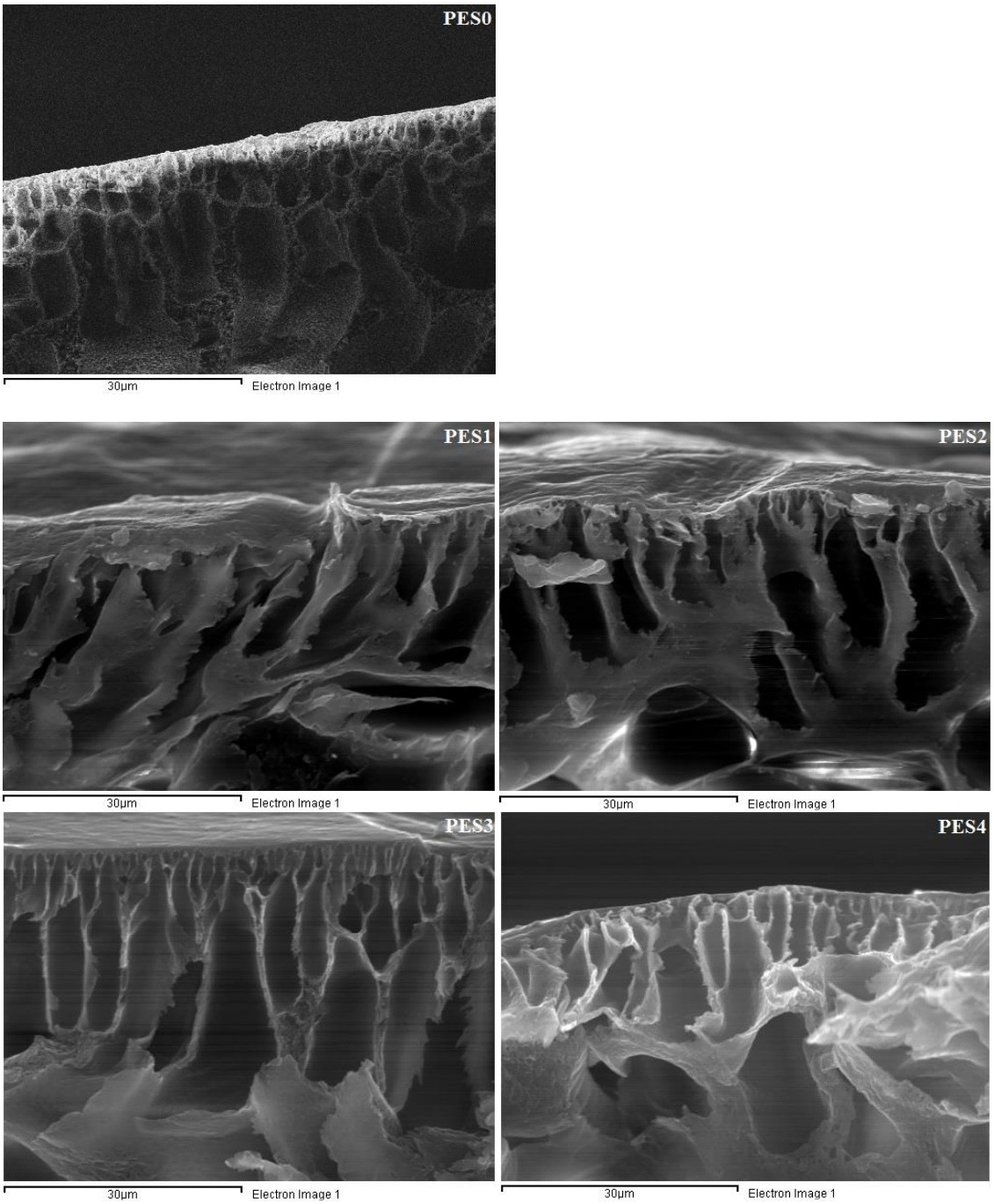

Fig. 4. Cross-section SEM images of the unmodified PES membrane (PES0), PES membranes photografted with Al_2O_3 (PES1 and PES2), and PES membranes photografted with PEG/Al_2O_3 (PES3 and PES4).

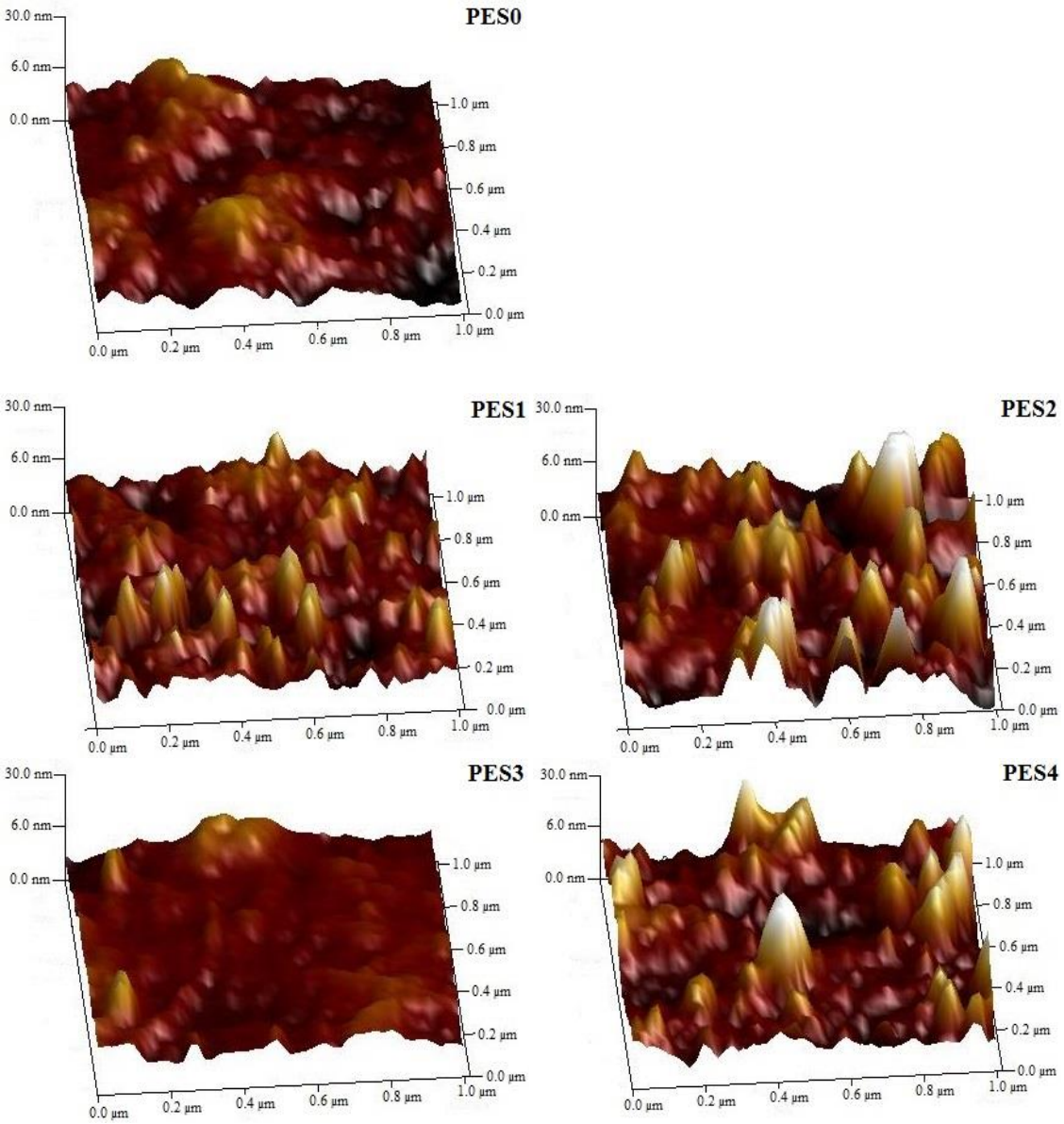

Fig. 5. Surface 3D AFM images of unmodified PES membrane (a) and PES membranes photografted: (b) with 0.5 wt% Al_2O_3, (c) with 1.0 wt% Al_2O_3, (d) with 2.0 wt% PEG and 0.5 wt% Al_2O_3, and (e) with 4.5 wt% PEG and 0.5 wt% Al_2O_3.

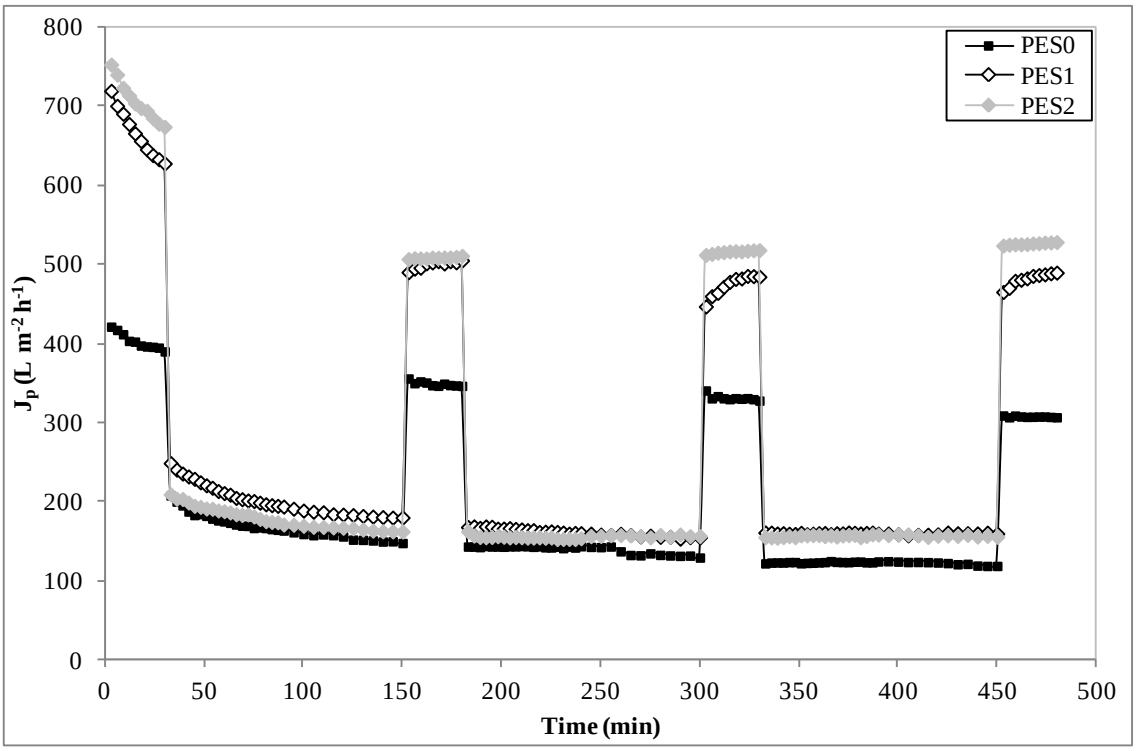

Fig. 6. Permeate flux versus filtration time for PES membranes with and without Al_2O_3 nanoparticles during membrane compaction with deionized water and three PEG fouling/rinsing cycles (25 ºC, 200 kPa).

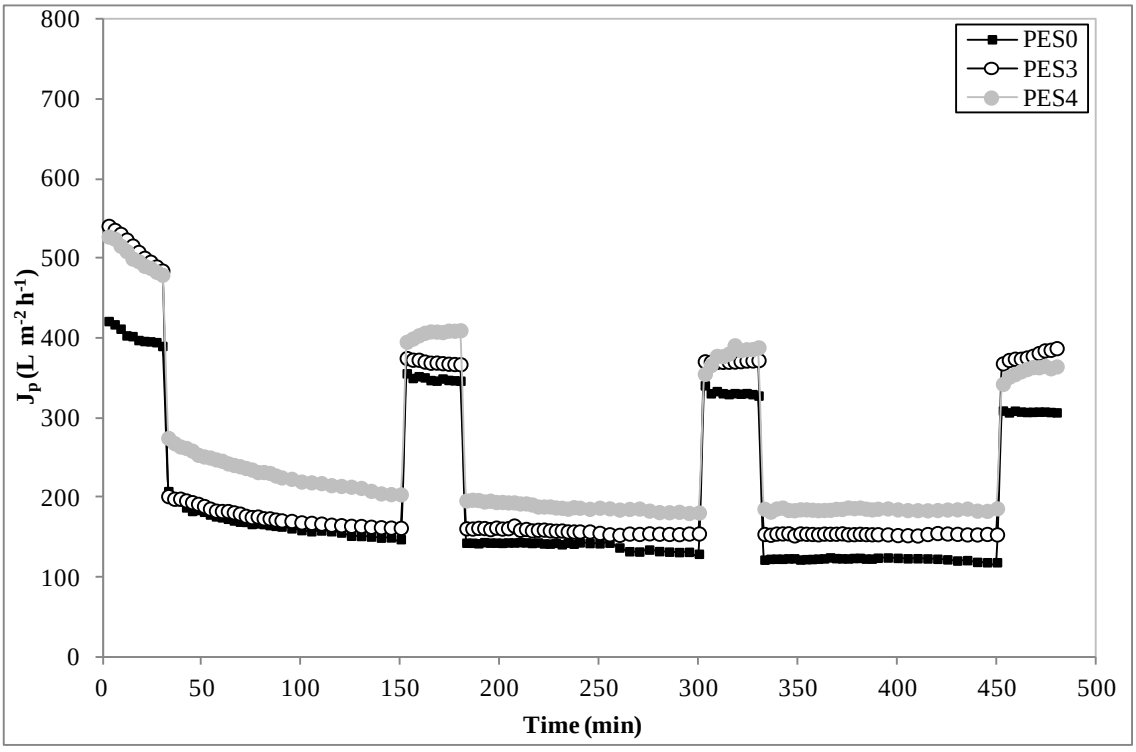

Fig. 7. Permeate flux versus filtration time for PES membranes with and without PEG/Al_2O_3 nanoparticles during membrane compaction with deionized water and three PEG fouling/rinsing cycles (25 ºC, 200 kPa).

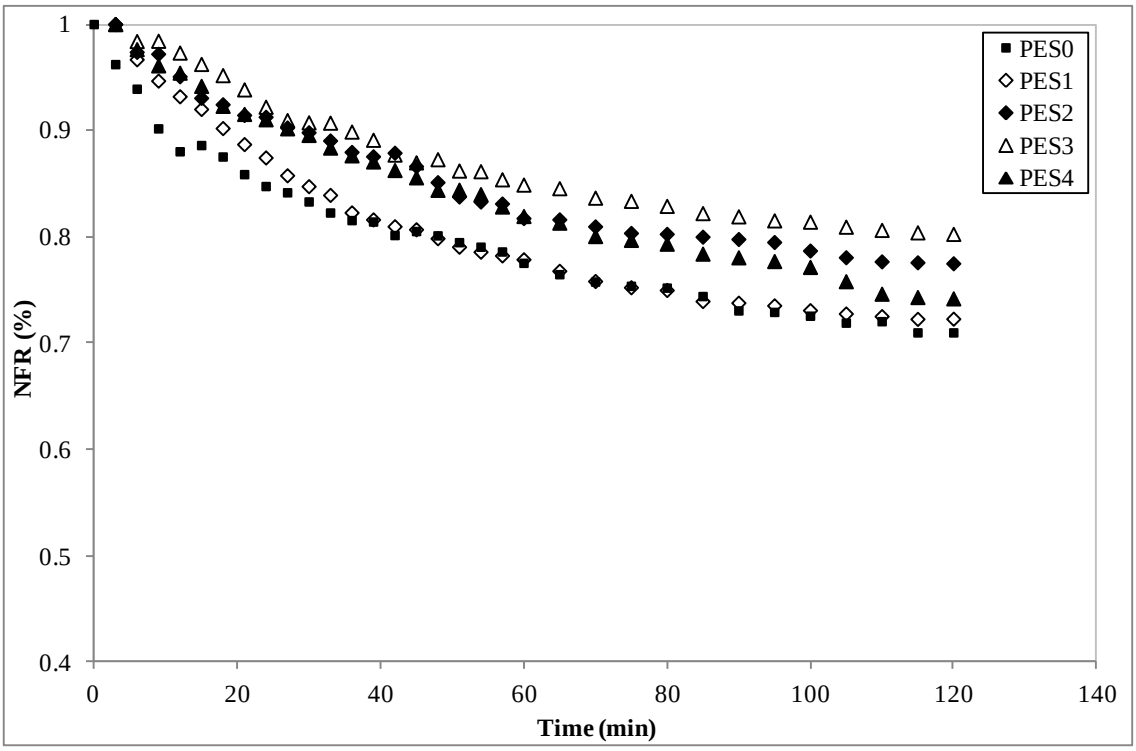

Fig. 8. Normalized flux ratio (NFR) in PEG ultrafiltration of different PES membranes with and without PEG/Al_2O_3 nanoparticles (25 ºC, 200 kPa).

Table 1. Degree of grafting (DG), water contact angle (WCA), membrane porosity (ε), equilibrium water content (EWC), average pore radius (r_m) and surface roughness of unmodified PES membrane (PES0) and membranes photomodified with different PEG/Al_2O_3 concentration

Membrane	Additive composition (wt%)		DG (μg cm^{-2})	WCA (º)	ε (%)	EWC (%)	r_m (nm)	Surface roughness (nm)	
	Al_2O_3	PEG						S_a	S_q
PES0	---	---	---	72.9±1.5	69.1±0.3	68.5±0.4	14.3±0.2	3.4±0.4	4.4±0.4
PES1	0.50	---	287.8±16.4	59.8±2.0	71.5±0.3	70.9±0.5	9.5±0.4	3.6±0.6	4.7±0.7
PES2	1.00	---	378.5±10.7	49.9±2.1	72.0±0.4	71.4±0.5	9.4±0.3	8.4±1.7	11.6±2.3
PES3	0.50	2.00	494.1±40.2	53.9±1.9	73.5±0.3	72.9±0.6	10.2±0.4	3.9±0.6	5.1±0.8
PES4	0.50	4.50	553.1±26.6	51.9±1.6	74.6±0.5	74.0±0.6	10.6±0.6	7.3±1.8	9.6±2.4

Table 2. EDX results for PES membranes photomodified with different PEG/Al_2O_3 concentration

Sample	Element							
	C K		S K		O K		Al K	
	wt%	at%	wt%	at%	wt%	at%	wt%	at%
PES0	23.20	29.52	6.00	2.86	70.80	67.62	0.00	0.00
PES1	25.00	31.22	3.32	1.56	71.62	67.18	0.06	0.03
PES2	23.46	29.73	5.52	2.66	70.89	67.54	0.14	0.08
PES3	26.05	32.20	1.82	0.85	72.12	66.94	0.01	0.01
PES4	25.87	32.04	2.04	0.96	72.03	66.94	0.06	0.03

Table 3. Hydraulic permeability, membrane intrinsic resistance and solute rejection for PEG of 10000, 20000 and 35000 g mol^{-1} for all the membranes tested

Membrane	Hydraulic permeability (L m^{-2} h^{-1} kPa^{-1})	Membrane resistance $\cdot 10^{-12}$ (m^{-1})	$R_{PEG\ 35}$ (%)	$R_{PEG\ 20}$ (%)	$R_{PEG\ 10}$ (%)
PES0	2.352	1.702	90.4±0.7	74.3±0.6	70.5±1.5
PES1	2.571	1.567	91.6±0.5	75.6±1.5	71.5±0.8
PES2	2.666	1.511	99.0±1.1	83.3±1.7	76.4±0.7
PES3	3.145	1.279	93.7±0.6	79.5±1.7	76.2±1.1
PES4	3.575	1.127	96.5±1.4	77.9±0.9	74.4±1.2

Membrane area = 100 cm^2; Temperature = 25 ºC.